THE JOURNAL OF PHYSICAL CHEMISTRY A

pubs.acs.org/JPCA Article

Atmospheric Chemistry of Methyl Isocyanide—An Experimental and Theoretical Study

Simen Gjelseth Antonsen, Arne Joakim C. Bunkan, Tomas Mikoviny, Claus J. Nielsen,* Yngve Stenstrøm, Armin Wisthaler, and Erika Zardin

Cite This: J. Phys. Chem. A 2020, 124, 6562–6571 Read Online

ACCESS | Metrics & More | Article Recommendations | Supporting Information

ABSTRACT: The reaction of CH_3NC with OH radicals was studied in smog chamber experiments employing PTR-ToF-MS and long-path FTIR detection. The rate coefficient was determined to be $k_{CH_3NC+OH} = (7.9 \pm 0.6) \times 10^{-11}$ cm^3 molecule^{-1} s^{-1} at 298 ± 3 K and 1013 ± 10 hPa; methyl isocyanate was the sole observed product of the reaction. The experimental results are supported by CCSD(T*)-F12a/aug-cc-pVTZ//M06-2X/aug-cc-pVTZ quantum chemistry calculations showing the reaction to proceed primarily via electrophilic addition to the isocyanide carbon atom. On the basis of the quantum chemical data, the kinetics of the OH reaction was simulated using a master equation model revealing the rate coefficient to be nearly independent of pressure at tropospheric conditions and having a negative temperature dependence with $k_{OH} = 4.2 \times 10^{-11}$ cm^3 molecule^{-1} s^{-1} at 298 K. Additional quantum chemistry calculations on the CH_3NC reactions with O_3 and NO_3 show that these reactions are of little importance under atmospheric conditions. The atmospheric fate of methyl isocyanide is discussed.

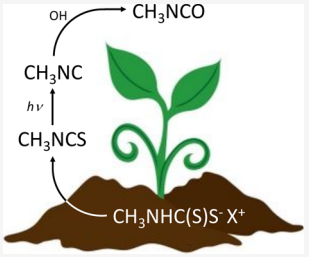

1. INTRODUCTION

Methyl isocyanide has been reported as a major product in the photolysis of methyl isothiocyanate,[1] the dominant breakdown product of commonly used soil fumigants based on *N*-methyldithiocarbamate.[2] Methyl isocyanide has also been suggested as a minor product in the atmospheric photo-oxidation of *N*-methyl methanimine,[3] which in turn is the major atmospheric photo-oxidation product of dimethyl- and trimethylamine.[3−5]

Very little is known about the atmospheric chemistry of the isocyanides. Alkyl isocyanides are generally not very soluble in water, but they are known to undergo hydrolysis in aqueous acidic solution to give primary amines and formic acid. For methyl isocyanide the pseudo-first-order rate coefficient for hydrolysis in weakly acidic solutions is around 10^{-3} s^{-1},[6] and hydrolysis on aqueous particles may present an important atmospheric loss process. A photoisomerization study of methyl isocyanide showed that the compound does not absorb at wavelengths longer than 260 nm,[7] and tropospheric photolysis is hence barred. No experimental rate coefficients are available for isocyanide gas-phase reactions, and the only relevant information appears in our recent quantum chemistry study of the atmospheric chemistry of CH_2═NH and HNC,[8] in which we obtained $k_{OH+HNC} = 1.3 \times 10^{-11}$ cm^3 molecule^{-1} s^{-1} from master equation calculations under atmospheric conditions.

2. EXPERIMENTAL AND COMPUTATIONAL METHODS

2.1. Experimental Methods. The experiments were performed in synthetic air (PRAXAIR 5.0) at 295 ± 2 K and 1013 ± 50 mbar in a 250 L electropolished stainless-steel reactor. The kinetic studies of the CH_3NC reactions with OH radicals were carried out by the relative rate method in a static gas mixture, in which the removal of the reacting species are measured simultaneously as a function of reaction time. Assuming that the compounds under study react solely with OH and that none of the compounds are reformed in any side reactions, the relative rate coefficient, k_{rel}, is given according to the following expression:

$$\ln\{[CH_3NC]_0/[CH_3NC]_t\} = k_{rel}\cdot\ln\{[Ref]_0/[Ref]_t\};\ k_{rel} = k_{CH_3NC}/k_{Ref} \quad (I)$$

where $[CH_3NC]_0$, $[CH_3NC]_t$, $[ref]_t$ and $[ref]_t$ are the concentrations of methyl isocyanide and the reference compound at start and at the time t, respectively, and k_{CH_3NC} and k_{ref} are the corresponding rate coefficients for their reactions with the radical in question. A plot of $\ln\{[CH_3NC]_0/[CH_3NC]_t\}$ vs $\ln\{[ref]_0/[ref]_t\}$ will thus give the relative reaction rate coefficient $k_{rel} = k_{CH_3NC}/k_{ref}$ as the slope.

The OH radicals were generated by photolysis of isopropyl nitrite (IPN) employing two Philips TLD-08 18 W

Received: June 6, 2020
Revised: July 14, 2020
Published: July 14, 2020

fluorescence lamps ($\lambda_{max} \sim 370$ nm) inserted in a quartz tube mounted into the reaction chamber.

$$CH_3CH(ONO)CH_3 + h\upsilon \rightarrow CH_3CH(\dot{O})CH_3 + NO \quad (1)$$

$$CH_3CH(\dot{O})CH_3 + O_2 \rightarrow CH_3C(O)CH_3 + HO_2 \quad (2)$$

$$HO_2 + NO \rightarrow OH + NO_2 \quad (3)$$

The photostability of methyl isocyanide toward the lamp output in clean air was investigated in separate experiments of around 2 h duration: no photoisomerization and no direct photolysis of the compound was detected by FTIR.

The stability of methyl isocyanide in the chamber clean air was investigated in separate experiments. Assuming the apparent sample loss to be of first order, a rate coefficient of $<10^{-5}$ s^{-1} was obtained. This corresponds to a lifetime of >24 h in the chamber, and the "natural" chamber loss of methyl isocyanide will therefore not impact the kinetic analyses, see below.

FT-IR. The Oslo Smog Chamber is equipped with a Bruker IFS-66v/S FTIR spectrometer coupled with a White multi-reflection mirror system for in situ analysis adjusted to give an optical path length of 120 m. FTIR spectra were recorded every 10 min by coadding 32 interferograms with a spectral resolution of 1 cm^{-1}. Boxcar apodization was used in the Fourier transformation.

Infrared spectra of the pure gas at 295 ± 2 K were recorded in the region of 4000−400 cm^{-1} by employing a nominal resolution of 1.0 cm^{-1} and Boxcar apodization of the interferograms. An DTGS detector was used to ensure optical linearity. The pressures of CH_3NC in a gas cell of 9.9 ± 0.2 cm, equipped with windows of KBr, ranged from 5 to 25 hPa and were measured using a CERAVAC CTR 100 pressure transducer with a stated accuracy of ±0.2% of reading. The transducer is calibrated for N_2 gas, but the accuracy of reading is trusted to be better than ±2% for other gases. Conservative estimates of systematic errors are pressure measurements (2%), path length (2%), temperature (1%), and definition of the baseline in integration procedures (2%).

Proton-Transfer-Reaction Time-of-Flight Mass Spectrometer (PTR-ToF-MS). A commercial PTR-TOF 8000 instrument (Ionicon Analytik GmbH, Innsbruck, Austria) was used for online organic trace gas measurements.[9] The instrument was operated at 100 Td (1 Td = 10^{-17} V cm^{-2} $molecule^{-1}$) in a 5 s integration mode; the drift tube was kept at a temperature of 50 °C and a pressure of 2.8 mbar. The analyzer was interfaced to the Oslo chamber via a 150 cm 1/8 in. SS tube (ID ∼ 2 mm) inside the FTIR chamber followed by 60 cm of 1/16 in. PEEK line, 1 mm inner diameter. The inlet flow was set to 300 sccm.

Instrumental Data Analysis. The spectra collected by the PTR-ToF-MS were analyzed with PTR-MS Viewer ver. 3.2.14 (Ionicon Analytik GmbH, Innsbruck, Austria). The mass scale of the spectra was consistently aligned with a three-point calibration using a permanent internal reference substance (1,2-diiodobenzene, CAS RN 615-42-9). Multiple peaks were manually fitted in the software to maximize the accuracy of the resulting signals in counts per second (cps).

Chemicals. Furan (Aldrich, > 99%), (R)-(+)-limonene (Sigma-Aldrich, 97%), α-pinene (Sigma-Aldrich, 98%), 2-propanol (VWR, Normapur), and sodium nitrite (Sigma-Aldrich, ReagentPlus, ≥ 99%) were used without further purification. 2-Propyl nitrite (isopropyl nitrite, IPN) was synthesized from 2-propanol, conc. hydrochloric acid, and sodium nitrite, and it was purified by repeatedly washing it with ice water.

Methyl isocyanide (CAS RN 593-75-9) was prepared following a procedure by Schuster, Scott, and Casanova with minor modifications.[10] A flask was equipped with a receiver flask. Quinoline (18 g, 0.14 mol) and *p*-toluensulfonyl chloride (10 g, 0.052 mol) were added to the flask. The receiver flask was cooled on a dry-ice/acetone bath, and then the system is heated to 75 °C and pressure is reduced to 10−15 Torr. *N*-Methylformamide (2.0 g, 0.034 mol) was added dropwise through a rubber septum while it was vigorously stirred, giving a colorless liquid condensing in the receiver trap. For further purification, the collected material was distilled at atmospheric pressure. At 59−60 °C, methyl isocyanide (0.89 g, 0.022 mol, 64% reaction yield) was collected as a colorless liquid. The ^1H and ^{13}C NMR spectra (see Figures S1 and S2 in the Supporting Information) proved the purity to be >95%. ^1H NMR (400 MHz, $CDCl_3$) δ 3.12 (s, 3H, CH_3); ^{13}C NMR (100 MHz, $CDCl_3$) δ 26.84 (CH_3), 156.68 (C). A quantitative IR spectrum of CH_3NC is presented in Figure S3.

2.2. Quantum Chemical Methods. Geometry optimization and vibrational frequency analysis of stationary points on the potential energy surfaces (PES) of the OH, NO_3, and O_3 reactions with CH_3NC were performed using the hybrid meta-GGA exchange-correlation M06-2X density functional.[11] Saddle points on the PESes of reactions were located by scanning the bonds formed/broken and subsequently validated in intrinsic reaction coordinate (IRC) calculations.[12]

All M06-2X reported results were obtained with tight optimization criteria and ultrafine integration grids. Additional B3LYP,[13−16] BHandHLYP (as implemented in Gaussian),[17] B98,[18] and MP2[19] calculations were carried out for the O_3 and NO_3 reactions. Energies of the stationary points were improved by explicitly correlated coupled cluster calculations with scaled triples contributions, denoted CCSD(T*)-F12a.[20,21] Dunning's correlation-consistent aug-cc-pVTZ basis set[22,23] was employed in all calculations. Reaction enthalpies were calculated using the G4 composite method.[24] The M06-2X, B3LYP, BHandHLYP, B98, MP2, and G4 calculations were performed in Gaussian09,[17] and the coupled cluster calculations were performed in Molpro 2012.1.[25,26]

2.3. Kinetics Calculations. Master equation calculations were carried out using the program MESMER 3.0[27] (Master Equation Solver for Multi-Energy-well Reactions) to simulate the kinetics of the OH radical reactions with CH_3NC as well as some consecutive reactions as previously described in our study of the OH + HNC reaction.[8] Spin−orbit coupling in the OH radical (139.7 cm^{-1})[28] was included in the model by lowering the energy of the OH radical with half of the splitting and including the $^2\Pi_{3/2}$ and $^2\Pi_{1/2}$ spin−orbit states in the electronic partition function. It was assumed that spin−orbit coupling could be neglected in prereaction adducts and in the saddle points.

Lennard-Jones parameters for the CH_3NC−OH system were approximated with values for CH_3CN (ε/k_B = 380 K, σ = 4.47 Å),[29] and the energy transfer in collisions with N_2 and O_2, $<\Delta E_{down}>$, was set to 250 cm^{-1}.

3. RESULTS AND DISCUSSION

3.1. Experimental. Methyl isocyanide was introduced to the smog chamber in a stream of clean air. Figure S3 in the

https://dx.doi.org/10.1021/acs.jpca.0c05127
J. Phys. Chem. A 2020, 124, 6562−6571

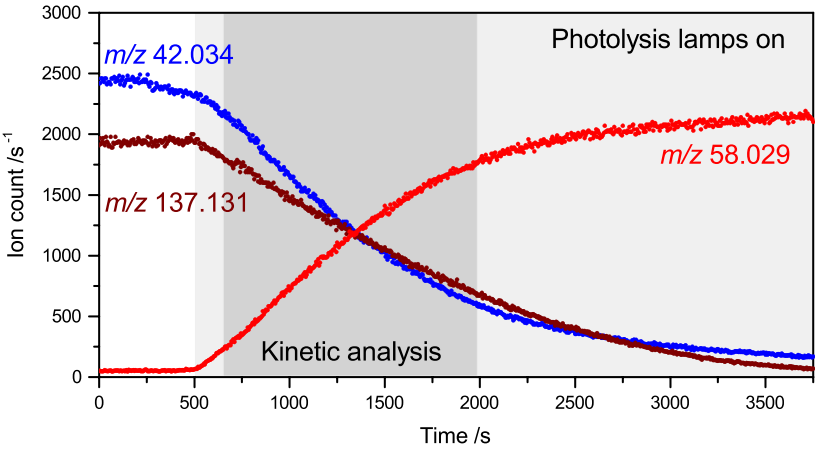

Figure 1. Decays of methyl isocyanide (m/z 42.034) and α-pinene (m/z 137.131) in the presence of OH radicals, and growth of methyl isocyanate (m/z 58.029) plotted as a function of time. The light gray shaded area indicates photolysis lamps being active; the dark gray shaded area indicates the time span of data employed in the kinetic analysis.

Supporting Information shows that the obtained IR spectrum conforms with the literature, and that there are no indications of the isomer, acetonitrile, as impurity.[30] Upon gas-phase protonation in the PTR instrument, only minor fragmentation takes place, and correlated ion signals were observed by PTR-ToF-MS at m/z 15.024 (CH_3^+) and 42.034 ($C_2H_4N^+$). Quantification of methyl isocyanide in the chamber was not pursued.

3.1.1. Kinetics of the CH_3NC + OH Reaction. Relative rate experiments were carried out employing furan, limonene, and α-pinene as the reference compounds and IPN as OH radical precursor. The experiments were monitored by PTR-ToF-MS, and typical mixing ratios in clean air were below 200 ppbV for the reactants and 1 ppmV for IPN. No additional NOx was added to the chamber.

Figure 1 illustrates the ion counts registered during a relative rate experiment using α-pinene as the reference compound; the other experiments proceeded in much the same way. The time span selected for kinetic analysis stretches ~30 min, and the average OH concentration during this period is ~8.6×10^6 cm^{-3}.

Figure 2 summarizes the data from the relative rate experiments that were analyzed according to equation I allowing a nonzero offset using a weighted least-squares procedure that includes uncertainties in both reactant concentrations.[31] The estimated uncertainties in the relative concentrations were taken as 1%. The analyses showed negligibly small intercepts and $k_{OH+furan}/k_{OH+CH_3NC}$ = 2.145 ± 0.025, $k_{OH+limonene}/k_{OH+CH_3NC}$ = 0.494 ± 0.009, and $k_{OH+\alpha\text{-pinene}}/k_{OH+CH_3NC}$ = 1.369 ± 0.010 (2σ errors from the statistical analyses). Taking today's recommended rate coefficients for the reference compounds at 298 K ($k_{OH+furan}$ = 4.0×10^{-11} cm^3 $molecule^{-1}$ s^{-1}, $\Delta log\ k = \pm 0.33$), limonene ($k_{OH+limonene}$ = 1.65×10^{-10} cm^3 $molecule^{-1}$ s^{-1}, $\Delta log\ k = \pm 0.12$), and α-pinene ($k_{OH+\alpha\text{-pinene}}$ = 5.3×10^{-11} cm^3 $molecule^{-1}$ s^{-1}, $\Delta log\ k = \pm 0.20$)[32] places the absolute rate for the CH_3NC + OH reaction at respectively 8.6 ± 2.8, 8.2 ± 1.0 and (7.3 ± 1.5) × 10^{-11} cm^3 $molecule^{-1}$ s^{-1} at 298 K. The statistical errors in the experimental relative rates are an order of magnitude smaller than the uncertainty estimates of the absolute rate coefficients for the reference compounds, and can be ignored in the error propagation. The spread in the absolute results is within their uncertainty estimates, and we suggest the weighted average with 2σ error, k_{OH+CH_3NC} = (7.9 ± 0.6) × 10^{-11} cm^3 $molecule^{-1}$ s^{-1} at 298 K, as our best estimate.

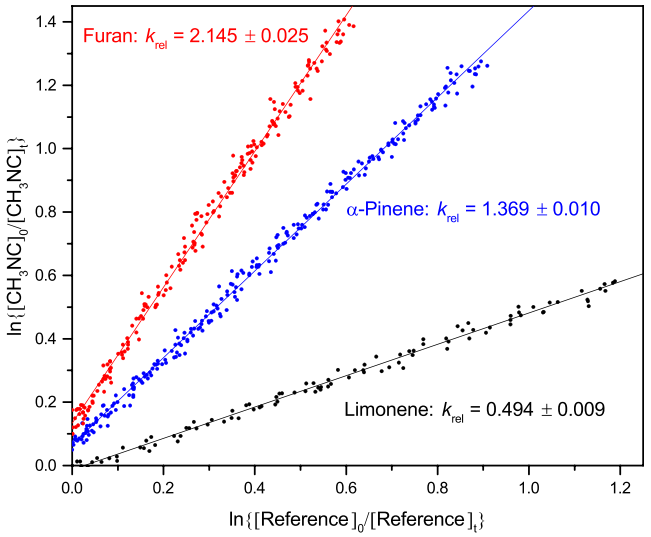

Figure 2. Decays of methyl isocyanide, furan, limonene, and α-pinene in the presence of OH radicals plotted as ln{[methyl isocyanide]$_0$/[methyl isocyanide]$_t$} vs ln{[furan]$_0$ /[furan]$_t$}, ln{[limonene]$_0$ /[limonene]$_t$}, and ln{[α-pinene]$_0$ /[α-pinene]$_t$}, respectively. The curves have been shifted along the y-axis for the sake of clarity. Uncertainties represent 2σ from the statistical analyses.

A product study showed methyl isocyanate, CH_3NCO (identified by the MS ion-signal of CH_3NCOH^+ at m/z 58.029), as the only product. No trace of the expected product resulting upon C−H abstraction—formyl isocyanide, CH(O)-NC—was detected at m/z 56.014 in the experiments. The proton affinity of formyl isocyanide is computed in G4-calculations to be 778 kJ mol^{-1} compared with, respectively, 691, 769, and 838 for H_2O, CH_3NCO, and CH_3NC, and with a calculated dipole moment of ~2.3 D the instrument sensitivity toward formyl isocyanide is estimated to be ~70% that of methyl isocyanide. Fragmentation of protonated formyl isocyanide resulting in HCN and HCO^+, is calculated with a barrier of ~30 kJ mol^{-1}. Assuming equipartitioning of the proton transfer reaction enthalpy, this is just below internal energy of $CHONCH^+$ in *statu nacendi*, and a significant

https://dx.doi.org/10.1021/acs.jpca.0c05127
J. Phys. Chem. A 2020, 124, 6562−6571

fragmentation is therefore expected. Unfortunately, the ion signals for HCO^+ and $^{15}N^{14}N^+$ cannot be resolved with the present instrumentation.

3.2. Computational. The M06-2X functional has been endorsed for the study of main-group thermochemistry and kinetics.[11] Of the molecular species included in the present study only the OH radical is included in the databases used for validating the M06-2X functional performance.

3.2.1. OH. The M06-2X results equate well with experiments. The OH distance of 0.972 Å is close to the experimental equilibrium value of 0.970.[33] The calculated dipole moment of 1.692 D compares with 1.721 ± 0.029,[34] and the fundamental mode is 5% higher than observed,[33] in which scaling by 0.956[35] causes a reduction to a 1% deviation.

3.2.2. NO_3. The NO_3 radical remains a computational challenge. The electronic ground state has D_{3h} symmetry ($\tilde{X}^2A_2'$).[36,37] HF calculations, however, locate three distinct minima: two C_{2v} structures having respectively 2 short and 1 long NO distance ($2s1l$), and 1 short and 2 long NO distances ($1s2l$), which are both lower in energy than the D_{3h} structure.[38] In contrast, MP2 calculations place the D_{3h} structure lower in energy than the two C_{2v} structures; even CCSD(T) cannot completely overcome the symmetry breaking of the reference function and still three solutions with slightly different energies are found.[38] Several frequently employed DFT methods, such as the B3LYP and B98 functionals, predict D_{3h} structures as global minima, whereas others, including M06-2X and BHandHLYP, also show symmetry breaking. The M06-2X hybrid functional locates the D_{3h} structure as a saddle point and the two C_{2v} structures as local energy minima.[39] BHandHLYP calculations also locate the D_{3h} structure as a saddle point and the ($2s1l$) C_{2v} structure as a minimum; the ($1s2l$) C_{2v} structure is found to be a saddle point. Table S1 in the Supporting Information summarizes the results obtained for the D_{3h} and the two C_{2v} structures. The vibrational fundamentals of the NO_3 radical obtained in B3LYP and B98 calculations are summarized in Table S2 in the Supporting Information.

The internally consistent M06-2X, BHandHLYP, MP2, G4 and CCSD(T*)-F12a electronic energies of the NO_3 radical were obtained by combining the theoretical results for the OH + HNO_3 → H_2O + NO_3 reaction, the standard enthalpies of formation at 298.15 K from the NIST-JANAF Themochemical Tables for OH (38.99 ± 1.21 kJ mol^{-1}), H_2O (−241.826 ± 0.042 kJ mol^{-1}), NO_3 (71.13 ± 20.9 kJ mol^{-1}), and HNO_3(−134.31 ± 0.42 kJ mol^{-1})[40] and the experimental fundamental modes of vibration for NO_3 (1050 a_1', 762.3 a_2'', 1492.4 e′, 360 e′ cm^{-1}).[41] The results are summarized in Table S3 in the Supporting Information. Note the inherent uncertainty of ∼21 kJ mol^{-1} in the experimental $\Delta_f H^0_{gas}$ for the NO_3 radical.[40]

The experimental NO distance in the NO_3 radical is 1.238 Å (r_0-structure);[42] the B3LYP and B98 results agree quite well with experiment predicting values of 1.232 and 1.231 Å, respectively. The calculated fundamental modes of vibration are, however, in less impressive agreement with experiment. In particular, the degenerate NO stretching and ONO bending modes are disturbingly lower than observed by respectively 400 and 150−200 cm^{-1} (see Table S2). Replacing the calculated fundamentals by the observed ones amounts to increases in the zero-point energies (ZPE) by +5.7 (B3LYP) and +7.4 (B98) kJ mol^{-1}.

3.2.3. O_3. Ozone is the textbook example of a molecule where multireference methods are needed to describe the electronic structure at a level that allows prediction of its physical properties akin to the experiments. The experimental structure, dipole moment, and vibrational fundamentals of ozone are extremely precisely determined (r_e = 1.27276 ± 0.00015 Å; α_e = 116.7542 ± 0.0025°),[43] μ = 0.533747 ± 0.000005 D,[44] and (ν_1 = 1103.13728 ± 0.00023, ν_2 = 700.931074 ± 0.000021, ν_3 = 1042.08398 ± 0.00023 cm^{-1}).[45,46] For comparison, MP2(Frozen Core) calculations result in OO distances that are slightly longer than the experimental value, but in an antisymmetric OO vibrational mode that is 1200 cm^{-1} higher than observed, and a dipole moment of 0.78 D. Coupled cluster methods are less sensitive to the HF wave function quality and show quite good agreement with experiment.[47] In general, the DFTs perform somewhat better. The M06-2X calculations, however, give r = 1.2316 Å, α = 118.31, μ = 0.7271 D, ν_1 = 1364.9, ν_2 = 791.5, and ν_3 = 1357.1 cm^{-1}, which can be characterized as distressingly off. Other commonly used DFTs such as B3LYP, BHandHLYP, and B98 give OO distances that are too short by 0.051 Å (BHandHLYP), 0.022 Å (B98), and 0.018 Å (B3LYP) and two OO stretching vibrations correspondingly calculated higher than observed by >200 cm^{-1} (BHandHLYP) and >100 cm^{-1} (B3LYP and B98). The DFT-methods mentioned also give similar incorrect dipole moments.

The DFT and MP2 shortcomings in describing the ozone electronic structure are exposed in Table 1, summarizing the CCSD(T*)-F12a electronic energies of the DTF and MP2 equilibrium structures relative to that obtained from the experimental equilibrium structure. Table 1 further contains the differences in the calculated and experimental ZPE based on the vibrational fundamentals. It can be seen that the bias introduced by blindfolded use of results from MP2 the DFTs amounts from +3.7 (B3LYP) to +16.7 (BHandHLYP) kJ mol^{-1}.

Table 1. Relative Electronic Energies (ΔE_{elec}) and Zero-Point Energies (ΔE_{ZPE}) in kJ mol^{-1} for O_3 with Reference to the Experimental Equilibrium Structure and the Experimental Fundamentals. Results from CCSD(T*)-F12a and QCM[a] Calculations Employing the aug-cc-pVTZ Basis Set

QCM	ΔE_{elec}	ΔE_{ZPE}
M06-2X	+7.8	+4.0
B3LYP	+1.7	+2.0
BHandHLYP	+12.4	+4.3
B98	+2.3	+2.6
MP2(FC)	+1.7	+7.8

[a]QMC, Quantum Chemistry Method.

3.2.4. CH_3NC. The CH_3NC structure obtained in M06-2X calculations agree well with the experimental equilibrium data (given in parentheses):[48] r_{C-H} = 1.087 Å (1.086), r_{C-N} = 1.420 (1.422), $r_{N\equiv C}$ = 1.162 (1.169), and α_{N-C-H} = 109.55° (109.47°). The calculated dipole moment, 3.85 D, is also in good agreement with the experimental value, 3.83 ± 0.06 D, from microwave spectroscopy.[49] The calculated structure and charge distribution are in harmony with the depiction: $H_3C—^+N\equiv C^-$.

https://dx.doi.org/10.1021/acs.jpca.0c05127
J. Phys. Chem. A 2020, 124, 6562−6571

Concerning the vibrational fundamentals, the calculated harmonic wavenumbers on the average fall 5% higher than the observations (13% for the CNC linear bending mode),[50] see Table S4 in the Supporting Information. Scaling by 0.956[35] brings the average deviation down to 2% (+7% for the CNC linear bending mode).

3.2.5. CH_3NC + OH. The reaction of CH_3NC with OH radicals can be initiated in two ways—either by C−H abstraction or by electrophilic addition to the π-system:

$$CH_3NC + OH \rightarrow CH_3N\dot{C}OH^{\ddagger} \quad \Delta H^0_{298\,K} = -120.5\ \text{kJ mol}^{-1} \tag{4a}$$

$$\rightarrow \dot{C}H_2NC + H_2O \quad \Delta H^0_{298\,K} = -92.8\ \text{kJ mol}^{-1} \tag{4b}$$

The reaction proceeds via prereaction complexes followed by inner, tight transition states. The structures of the prereaction complexes, PRE_{4a} and PRE_{4b}, are illustrated in Table S4. The OH radical is linearly H-bonded ($CH_3NC\cdots HO$) in PRE_{4a}; in PRE_{4b} the OH radical is rotated toward the CH_3-group and parallel the π-system. The barriers to reactions 4a and 4b are calculated to be −7.8 and +12.8 kJ/mol, respectively, indicating that the C−H abstraction route is of minor importance at tropospheric conditions, see below. Figure 3 shows the stationary points on the potential energy surfaces (PES) of the two reaction routes as resulting in CCSD(T*)-F12a/aug-cc-pVTZ//M06-2X/aug-cc-pVTZ calculations. Energies, the T_1[51] and D_1[52,53] diagnostics values, Cartesian coordinates, and vibration−rotation data are summarized in Table S4.

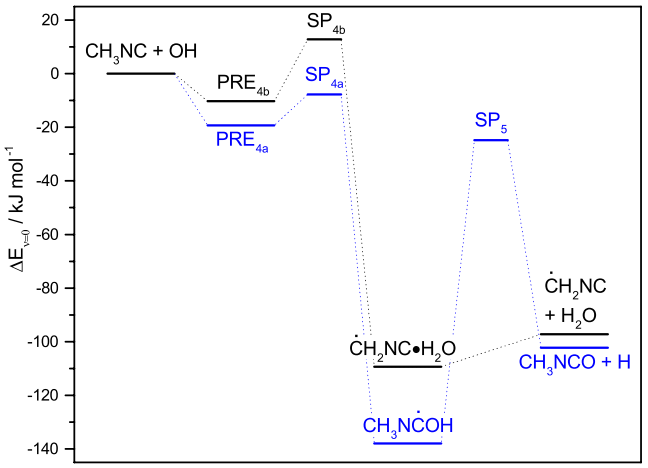

Figure 3. Stationary points on the potential energy surface of the CH_3NC + OH reaction. Results from CCSD(T*)-F12a/aug-cc-pVTZ//M02−2X/aug-cc-pVTZ calculations.

The $CH_3N\dot{C}OH$ radical, which is formed with a considerable amount of internal energy, may eject a hydrogen atom directly in analogy to the route found for the HNC + OH reaction:[8]

$$CH_3N\dot{C}OH^{\ddagger} \rightarrow CH_3NCO + H \quad \Delta H^0_{298\,K} = 20.8\ \text{kJ mol}^{-1} \tag{5}$$

Other possible fates of the $CH_3N\dot{C}OH$ radical include reaction with O_2, either in a direct hydrogen abstraction or via the formation of an intermediate peroxy-radical:

$$CH_3N\dot{C}OH + O_2 \rightarrow CH_3NCO + HO_2 \quad \Delta H^0_{298\,K} = -185.7\ \text{kJ mol}^{-1} \tag{6a}$$

$$\rightarrow CH_3NC(O\dot{O})OH^{\ddagger} \quad \Delta H^0_{298\,K} = -182.0\ \text{kJ mol}^{-1} \tag{6b}$$

$$CH_3NC(O\dot{O})OH \rightarrow CH_3NCO + HO_2 \quad \Delta H^0_{298\,K} = -3.6\ \text{kJ mol}^{-1} \tag{7}$$

The PES for O_2 approaching $CH_3N\dot{C}OH$ apparently targets peroxy-radical formation, and we were unsuccessful in pinpointing a direct H-abstraction route. The M06-2X/aug-cc-pVTZ calculations locate a saddle point (SP_{6b}) with a small barrier of +3.2 kJ mol^{-1} to reaction 6b. This is likely an artifact of the functional as the high correlation calculations place the energy of this structure below the entrance energy of the reactants. The T_1 and D_1 diagnostic values for the single point CCSD(T) calculation are worryingly large, and the results for SP_{6b} should be considered with some reservation (for the sake of completeness, the "saddle point" is included in the documentation). Figure 4 shows the energies of the stationary points on the PES of the $CH_3N\dot{C}OH$ + O_2 reaction. The underlying quantum chemistry data are collected in Table S5 in the Supporting Information.

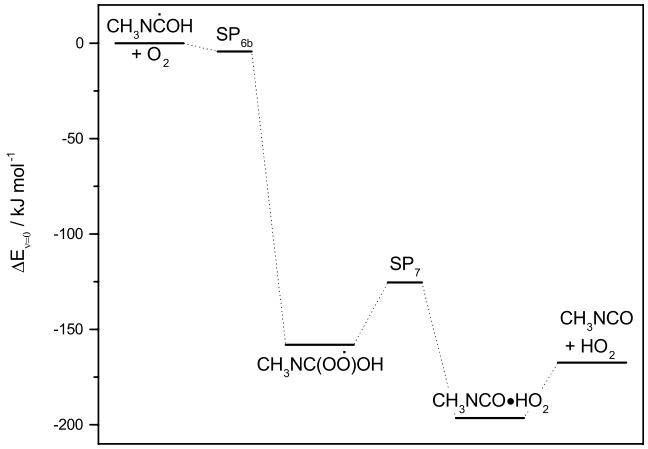

Figure 4. Stationary points on the potential energy surface of the CH_3NCOH + O_2 reaction. Results from CCSD(T)-F12a/aug-cc-pVTZ//M02−2X/aug-cc-pVTZ calculations.

It is obvious that $CH_3N\dot{C}OH$ radicals will react fast with O_2 forming an activated intermediate peroxy-radical $CH_3NC(O\dot{O})OH^{\ddagger}$, which may then undergo unimolecular rearrangement followed by loss of HO_2 to form CH_3NCO. The lifetime of $CH_3NC(O\dot{O})OH$ was investigated in a master equation model based on the PES illustrated in Figure 4. The lifetime was calculated to be $<10^{-6}$ s at atmospheric conditions, which is too short for any competing bimolecular reaction with species such as NO or other $R\dot{O}O$ radicals.

The $\dot{C}H_2NC$ radical, formed in reaction 4b, is expected to follow the reaction routes established for alkyl radicals. That is, the major product will be formyl isocyanide:

$$\dot{C}H_2NC + O_2 \rightarrow \dot{O}OCH_2NC \quad \Delta H^0_{298\,K} = -100.1\ \text{kJ mol}^{-1} \tag{8}$$

https://dx.doi.org/10.1021/acs.jpca.0c05127
J. Phys. Chem. A 2020, 124, 6562−6571

$$\dot{O}OCH_2NC + NO \rightarrow \dot{O}CH_2NC + NO_2$$
$$\Delta H^0_{298\,K} = -67.1\ \text{kJ mol}^{-1} \quad (9)$$

$$\dot{O}CH_2NC + O_2 \rightarrow CHONC + HO_2$$
$$\Delta H^0_{298\,K} = -138.3\ \text{kJ mol}^{-1} \quad (10)$$

In summary: the quantum chemistry calculations show that CH_3NC will react fast with OH radicals and that CH_3NCO is the dominant product in the reaction at atmospheric conditions.

3.2.5.1. Calculation of k_{CH_3NC+OH}. Rate coefficients for the reaction of CH_3NC with OH radicals were calculated using a master equation model based on the PES illustrated in Figure 3. The internal rotations of the CH_3-group in the saddle point to $CH_3N\dot{C}OH$ formation (SP_{4a}), in $CH_3N\dot{C}OH$, in the H-ejection saddle point (SP_5), and in CH_3NCO were treated explicitly employing the rotational potentials obtained in M06-2X/aug-cc-pVTZ calculations. Also, the internal rotations of the OH-group in SP_{4a} and in $CH_3N\dot{C}OH$ were treated this way. Figures S4−S9 in the Supporting Information show the calculated rotational potentials.

The long-range transition state theory method (LRTST)[54] was used to estimate the capture rate coefficient for formation of the prereaction complex: $k_{capture}(T) = 7.2 \times 10^{-10}(T/298)^{-1/6}$ cm^3 $molecule^{-1}$ s^{-1}. Reaction 5 was treated as an irreversible sink, and reactions 6−7 were included as a simple bimolecular loss term with $k_{O_2} = 10^{-12}$ cm^3 $molecule^{-1}$ s^{-1}. Tunneling was included for reactions 4a, 4b and 5 using a one-dimensional asymmetric Eckart potential.[55]

The model predicts a negative temperature dependence of the reaction with $k_{abstraction} = 4.3 \times 10^{-14}$ cm^3 $molecule^{-1}$ s^{-1} being 3 orders of magnitude slower than $k_{addition} = 4.2 \times 10^{-11}$ cm^3 $molecule^{-1}$ s^{-1} at 1 bar and 298 K, Figure S10 in the Supporting Information. There is a small pressure dependence amounting to around 5% at 298 K in going from 1000 to 10 mbar. The rate coefficients can be parametrized reasonably well by the Arrhenius equation and accurately by the modified Arrhenius equation in the range 200−400 K, see Figure S11 in the Supporting Information. The branching between direct H-ejection from $CH_3N\dot{C}OH$ and H-abstraction by O_2 varies with temperature and pressure and is around 30:70 at atmospheric conditions.

A sensitivity analysis shows the energy of the saddle point SP_{4a} to be the most important model parameter. A change in $\Delta E_{v=0}$ by ±2 kJ mol^{-1} results in changes of respectively −45 and +62% in k_{CH_3NC+OH}. Changes in the relative energy of PRE_{4a} by ±2 kJ mol^{-1} results in <1% change in k_{CH_3NC+OH}; the relative energies of the other stationary points on the PES have very little impact.

The effect of introducing scaled vibrational wavenumbers, without a simultaneous change in the zero-point energies, amounts to a 5% increase in k_{CH_3NC+OH}. Introducing the consistently scaled zero-point energies in the PES in addition to the wavenumber scaling increases k_{CH_3NC+OH} by 14%.

The model results are essentially insensitive to an order of magnitude variation in k_{O2}. Further, a 25% variation in the Lennard-Jones parameters and ±50 cm^{-1} variation in the collisional energy transfer $<\Delta E_{down}>$ resulted in changes of <1% in k_{CH_3NC+OH}. The LRTST value for $k_{capture}$ should be considered as an upper limit, and reducing $k_{capture}$ by a factor of 2 resulted in a 9% reduction in k_{CH_3NC+OH}. Tunneling increases the calculated rate coefficients by 5%; the major contribution is from the initial OH addition reaction 4a. Concerning the sensitivity to barrier heights to internal rotation, a ±50% change in barrier height to the internal rotation of OH in SP_{4a} changes the calculated rate coefficient by respectively −12 and +31%. The results are less sensitive to the rotational barrier of the CH_3-group in SP_{4a}, for which an order of magnitude variation results in a 6% change in k_{CH_3NC+OH}. The sensitivity to the other barrier heights is negligible—an order of magnitude variation in the barriers to internal rotation of the CH_3-groups in $CH_3N\dot{C}OH$, SP_5, and in CH_3NCO changes the model results by less than 1%. Similar variation in the OH rotation potential in $CH_3N\dot{C}OH$ results in changes <2%.

In summary, the calculated rate coefficients are essentially determined by the height of the inner, tight transition state associated with saddle-point SP4a. Lowering the calculated barrier height by 2.65 kJ mol^{-1} aligns the computed rate coefficients to the experimental value at 298 K, Figure 5. The

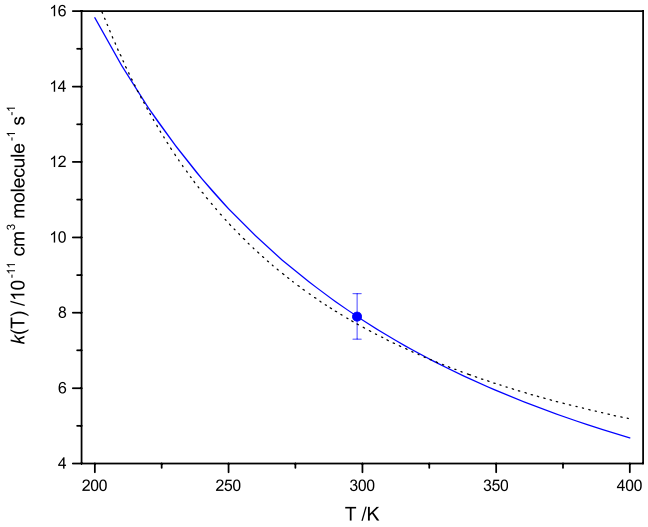

Figure 5. Experimental and aligned theoretical rate coefficients for the reaction of OH radicals with CH_3NC at 1013 bar. Blue curve: Calculated rate coefficients. Black dotted curve: Calculated rate coefficients fitted by the Arrhenius equation.

rate coefficients can be parametrized reasonably well by the Arrhenius equation in the range of 200−400 K, $k_{CH_3NC+OH}(T) = 1.63 \times 10^{-11} \times \exp(463/T)$, and accurately by the modified Arrhenius equation, $k_{CH_3NC+OH}(T) = 8.82 \times 10^{-11} \times (T/298)^{-1.88} \times \exp(-32.8/T)$ cm^3 $molecule^{-1}$ s^{-1}.

3.2.6. $CH_3NC + NO_3$. The $CH_3NC + NO_3$ reaction is found to proceed either via electrophilic addition to the isocyanide group resulting in methyl isocyanate or via H-abstraction:

$$CH_3NC + NO_3 \rightarrow CH_3NCO + NO_2$$
$$\Delta H^0_{298\,K} = -305\ \text{kJ mol}^{-1} \quad (11a)$$

$$\rightarrow \dot{C}H_2NC + HNO_3 \qquad \Delta H^0_{298\,K} = -19\ \text{kJ mol}^{-1} \quad (11b)$$

The quantum chemistry data for the reaction are collected in Table S6 in the Supporting Information. The calculations predict a barrier to reaction 11a ranging from ∼20 kJ mol^{-1} (B3LYP and B98) to ∼35 kJ mol^{-1} (CCSD(T*)-F12a//MP2). Notably, all five theoretical methods predict a much higher

https://dx.doi.org/10.1021/acs.jpca.0c05127
J. Phys. Chem. A 2020, 124, 6562−6571

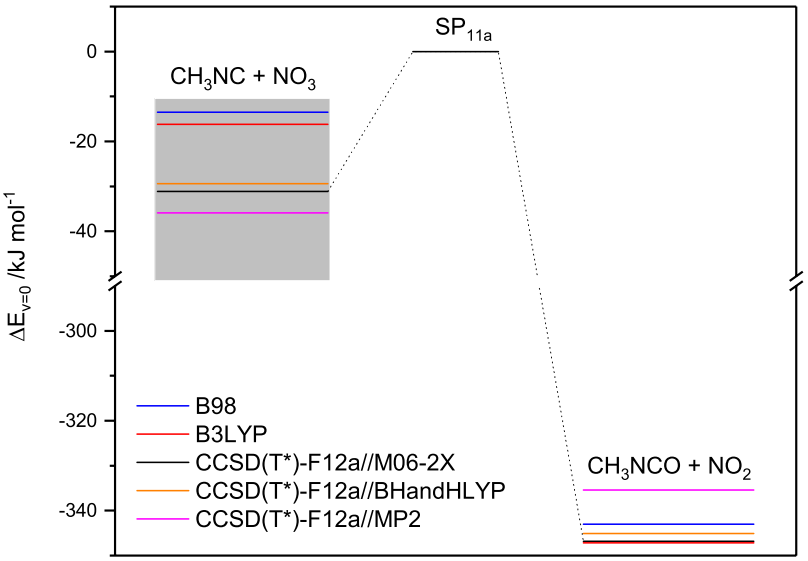

Figure 6. Stationary points on the potential energy surface of the $CH_3NC + NO_3$ reaction. Results from calculations employing the aug-cc-pVTZ basis set. The gray shaded box, centered around the CCSD(T*)-F12q//M06-2X energy of the reactants, illustrates the inherent uncertainty in the electronic energy of the NO_3 radical obtained in M06-2X, BHandHLYP, and MP2 calculations.

barrier to reaction 11b than to reaction 11a; the difference in barrier heights, obtained in the CCSD(T*)-F12a single point calculations, is around 30 kJ mol^{-1} for all methods employed.

Any electronic barrier to an NO_3 radical reaction with a compound will arise on a path between the reactant and a C_{2v}-like NO_3 radical structure (2*s*1*l*) on the entrance side and the product(s) on the exit side. This part of the PES can be characterized reasonably well by the methods employed, and it can therefore definitely be concluded that the H-abstraction reaction will not be relevant at atmospheric conditions.

The first part of the PES, connecting the electronic ground state of the NO_3 radical to the C_{2v}-like structure of the NO_3 radical in the activated reaction complex, cannot be described with the same degree of confidence. The M06-2X, BHandHLYP, MP2, and CCSD(T*)-F12a energies are all biased by a possible error in the experimental $\Delta_f H^0_{gas}$ for the NO_3 radical; the B3LYP and B98 energies cannot be improved by high-correlation single-point calculations without introducing the same bias as imposed on the other methods. Figure 6 illustrates the energies of stationary points of the PES obtained in the five models for reaction 11a. The B3LYP and B98 ZPE values for the NO_3 radical in Table S6 have, respectively, been corrected by +5.7 and +7.4 kJ mol^{-1}, see section 3.2.2.

The lowest barrier to reaction 11a is obtained with the B98 and B3LYP functionals. RRKM calculations, based on these results, give rate coefficients around respectively 7×10^{-18} and 3×10^{-17} cm^3 $molecules^{-1}$ s^{-1} at 298 K. Replacing the incorrectly calculated vibrational fundamentals of the NO_3 radical by the experimental values (and correcting the corresponding ZPE's) increases the calculated rate coefficients to respectively 2.5×10^{-16} and 4.6×10^{-16} cm^3 $molecules^{-1}$ s^{-1}.

3.2.7. $CH_3NC + O_3$. The reaction proceeds in accordance with the electronic structure by addition to the C atom of the isocyanide group resulting in methyl isocyanate:

$$CH_3NC + O_3 \rightarrow CH_3NCO + O_2(^1\Delta_g)$$
$$\Delta H^0_{298\ K} = -306\ \text{kJ mol}^{-1} \quad (12)$$

The M06-2X calculations indicate a single, relatively high barrier of around 50 kJ mol^{-1} to reaction 12, and the reaction should accordingly be very slow at atmospheric conditions.

The saddle point structure to reaction 12 warrants a multireference approach—the T_1 and D_1 diagnostic values for the CCSD(T) calculation are troublingly large. This is, however, outside the scope of the present study. The relative energies of the stationary points on the PES obtained in M06-2X, B3LYP, BHandHLYP, B98, and MP2 calculations on reaction 12 are compared in Table S7 in the Supporting Information. The barriers obtained in the five models span from 20 to 80 kJ mol^{-1}. However, for the present purpose the CCSD(T*)-F12a/aug-cc-pVTZ single point energies are essentially independent of the structure optimization method suggesting a barrier to reaction in the range 50−60 kJ mol^{-1}. A master equation calculation, based on the CCSD(T*)-F12a//M06-2X results, gives a rate coefficient around 5×10^{-25} cm^3 $molecules^{-1}$ s^{-1}. Replacing the incorrectly calculated O_3 properties by the experimental equilibrium values (see section 3.2.3) in the master equation-model results in a lowering of the rate coefficient to 8×10^{-26} cm^3 $molecules^{-1}$ s^{-1}.

4. CONCLUSIONS

Methyl isocyanide is shown in experiments and by quantum chemistry methods to react rapidly in the gas phase with OH radicals and slowly with NO_3 radicals and O_3; in all cases, CH_3NCO is the sole product observed/predicted. The quantum chemistry calculations show that the CH_3NC + OH reaction proceeds via a submerged barrier with computed rate coefficient of 4.2×10^{-11} cm^3 $molecule^{-1}$ s^{-1} at 298 K and 1013 hPa. The quantum chemistry calculations also imply that the $CH_3NC + NO_3$ and $CH_3NC + O_3$ reactions are slow with rate coefficients of less than 5×10^{-16} and 10^{-25} cm^3 $molecules^{-1}$ s^{-1} at 298 K, respectively.

The NO_3 radical concentrations are low during daylight hours, but can become elevated at night, and a 12-h night-time average concentration of $\approx 5 \times 10^8$ cm^{-3} have been proposed.[56,57] For a diurnal average NO_3 level of 5×10^8 molecules cm^{-3}, a compound will have a lifetime of 1 day with

https://dx.doi.org/10.1021/acs.jpca.0c05127
J. Phys. Chem. A 2020, 124, 6562−6571

respect to reaction with NO_3 if the corresponding rate coefficient is around 2.3×10^{-14} cm^3 molecules^{-1} s^{-1}. For CH_3NC, this would require the barrier to reaction 11a to be around 60% (10 kJ mol^{-1}) lower than obtained in the ZPE-corrected B3LYP and B98 calculations. Further, to align the B3LYP and B98 results with the CCSD(T)-F12a//QCM results (QCM = M06-2X, BHandHLYP, and MP2) will require $\Delta_f H^0_{gas}$ for the NO_3 radical to be more than 20 kJ mol^{-1} larger than the experimental value of 71.13 ± 20.9 kJ mol^{-1} at 298 K.[40] We consider this highly improbable and conclude that the $CH_3NC + NO_3$ reaction is too slow to be of importance under atmospheric conditions.

The empirical linear free energy relationship between rate coefficients for electrophilic OH and NO_3 radical addition reactions, $\log(k_{NO_3}) = (21.6 \pm 2) + (3.32 \pm 0.2) \times \log(k_{OH})$,[56] predicts $k_{NO_3+CH_3NC}$ to be very fast, ~1.1×10^{-12} cm^3 molecule^{-1} s^{-1}. Such a fast NO_3 reaction can only be realized if the barrier to reaction 11a is below the entrance energy of the reactants, which is completely incompatible with all the quantum chemistry results.

Assuming an average atmospheric ozone level of 10^{12} molecules cm^{-3} (~40 ppbV) a compound will have a lifetime of 1 day with respect to reaction with ozone if the corresponding rate coefficient is around 10^{-17} cm^3 molecules^{-1} s^{-1}. For CH_3NC, this would require the barrier to reaction 12 to be around 14.5 kJ mol^{-1}, and not around 60 kJ mol^{-1} as suggested in all our calculations. We consider an inaccuracy of such a magnitude as improbable and conclude that $CH_3NC + O_3$ reaction is too slow to be of importance under atmospheric conditions.

With an experimental room temperature rate coefficient for the $CH_3NC + OH$ reaction of 7.9×10^{-11} cm^3 molecule^{-1} s^{-1}, the atmospheric lifetime of CH_3NC will around 4 h for photochemical oxidation. The competing hydrolysis in/on acidic aqueous particles will therefore not be efficient enough to compete in general. The major product in atmospheric CH_3NC photo-oxidation is CH_3NCO, which, in contrast, has a long atmospheric lifetime of around 6 months.[58,59]

■ ASSOCIATED CONTENT

Supporting Information

The Supporting Information is available free of charge at https://pubs.acs.org/doi/10.1021/acs.jpca.0c05127.

^{1}H NMR of CH_3NC (Figure S1); ^{13}C NMR of CH_3NC (Figure S2); Infrared spectra of CH_3NC and CH_3CN (Figure S3); Potential to internal rotation of the CH_3-group in SP_{4a} (Figure S4); Potential to internal rotation of the OH moiety in SP_{4a} (Figure S5); Potential to internal rotation of the CH_3-group in $CH_3\dot{N}COH$ (Figure S6); Potentials to internal rotation of the OH moiety in $CH_3\dot{N}COH$ (Figure S7); Potential to internal rotation of the CH_3-group in SP_5 (Figure S7); Potential to internal rotation of the CH_3-group in CH_3NCO (Figure S8); Potential to internal rotation of the CH_3-group in CH_3NCO (Figure S9); Calculated $k_{CH3NC+OH}(T)$ at 1000, 100, and 10 mbar (Figure S10); Calculated $k_{CH3NC+OH}(T)$ and parametrization (Figure S11); Electronic energies and relative electronic energies for the NO_3 radical (Table S1), Fundamental modes of vibration in NO_3 (Table S2); Internally consistent energies of the NO_3 radical; HNO_3, H_2O and OH (Table S3); Quantum chemistry results for CH_3NC + OH (Table S4); Quantum chemistry results for $CH_3N\dot{C}OH + O_2$ (Table S5); Quantum chemistry results for $CH_3NC + NO_3$ (Table S6); Quantum chemistry results for $CH_3NC + O_3$ (Table S7) (PDF)

■ AUTHOR INFORMATION

Corresponding Author

Claus J. Nielsen − *Section for Environmental Sciences, Department of Chemistry, University of Oslo, 0315 Oslo, Norway;* orcid.org/0000-0002-2962-2634; Phone: +47 2285 5680; Email: claus.nielsen@mail.uio.no

Authors

Simen Gjelseth Antonsen − *Department of Chemistry, Biotechnology and Food Science, NO-1432 Aas, Norway;* orcid.org/0000-0002-9416-5476

Arne Joakim C. Bunkan − *Section for Environmental Sciences, Department of Chemistry, University of Oslo, 0315 Oslo, Norway*

Tomas Mikoviny − *Section for Environmental Sciences, Department of Chemistry, University of Oslo, 0315 Oslo, Norway*

Yngve Stenstrøm − *Department of Chemistry, Biotechnology and Food Science, NO-1432 Aas, Norway;* orcid.org/0000-0001-9598-5225

Armin Wisthaler − *Section for Environmental Sciences, Department of Chemistry, University of Oslo, 0315 Oslo, Norway;* orcid.org/0000-0001-5050-3018

Erika Zardin − *Section for Environmental Sciences, Department of Chemistry, University of Oslo, 0315 Oslo, Norway*

Complete contact information is available at: https://pubs.acs.org/10.1021/acs.jpca.0c05127

Notes

The authors declare no competing financial interest.

■ ACKNOWLEDGMENTS

This work is part of the Atmospheric Chemistry of Amines project (ACA) supported by the CLIMIT program under contract 244055 and has received additional support from the Research Council of Norway through its Centres of Excellence scheme, project number 262695.

■ REFERENCES

(1) Alvarez, R. A.; Moore, C. B. Quantum Yield for Production of CH_3NC in the Photolysis of CH_3NCS. *Science* **1994**, *263*, 205−207.

(2) Ajwa, H.; Ntow, W. J.; Qin, R.; Gao, S. In *Hayes' Handbook of Pesticide Toxicology*; Krieger, R., Ed.; Academic Press: New York, 2010; pp 315−330.

(3) Nielsen, C. J.; D'Anna, B.; Karl, M.; Aursnes, M.; Boreave, A.; Bossi, R.; Bunkan, A. J. C.; Glasius, M.; Hansen, A.-M. K.; Hallquist, M.; et al. *Atmospheric Degradation of Amines (ADA). Summary report: Photo-oxidation of methylamine, dimethylamine and trimethylamine.*; CLIMIT project no. 201604. Norwegian Institute for Air Research (NILU): Kjeller, Norway, 2011.

(4) Pitts, J. N.; Grosjean, D.; Vancauwenberghe, K.; Schmid, J. P.; Fitz, D. R. Photooxidation of Aliphatic Amines under Simulated Atmospheric Conditions - Formation of Nitrosamines, Nitramines, Amides, and Photochemical Oxidant. *Environ. Sci. Technol.* **1978**, *12*, 946−953.

(5) Lindley, C. R. C.; Calvert, J. G.; Shaw, J. H. Rate Studies of the Reactions of the $(CH_3)_2N$ Radical with O_2, NO, and NO_2. *Chem. Phys. Lett.* **1979**, *67*, 57−62.

(6) Yu-Yuan, L. *Acid Catalyzed Hydrolysis of Methyl Isocyanide*. Ph.D. Dissertation, Memorial University of Newfoundland, 1972.
(7) Dunning, B. K.; Shaw, D. H.; Pritchard, H. O. Photochemical Behavior of Isocyanides. *J. Phys. Chem.* **1971**, *75*, 580−581.
(8) Bunkan, A. J. C.; Tang, Y.; Sellevåg, S. R.; Nielsen, C. J. Atmospheric Gas Phase Chemistry of CH_2=NH and HNC. A First-Principles Approach. *J. Phys. Chem. A* **2014**, *118*, 5279−5288.
(9) Jordan, A.; Haidacher, S.; Hanel, G.; Hartungen, E.; Märk, L.; Seehauser, H.; Schottkowsky, R.; Sulzer, P.; Märk, T. D. A High Resolution and High Sensitivity Proton-Transfer-Reaction Time-of-Flight Mass Spectrometer (PTR-TOF-MS). *Int. J. Mass Spectrom.* **2009**, *286*, 122−128.
(10) Schuster, R. E.; Scott, J. E.; Casanova, J., Jr. Methyl Isocyanide. *Org. Synth.* **1966**, *46*, 75−77.
(11) Zhao, Y.; Truhlar, D. G. The M06 Suite of Density Functionals for Main Group Thermochemistry, Thermochemical Kinetics, Noncovalent Interactions, Excited States, and Transition Elements: Two New Functionals and Systematic Testing of Four M06-Class Functionals and 12 other Functionals. *Theor. Chem. Acc.* **2008**, *120*, 215−241.
(12) Fukui, K. The Path of Chemical Reactions - the IRC Approach. *Acc. Chem. Res.* **1981**, *14*, 363−368.
(13) Becke, A. D. Density-Functional Thermochemistry. III. The Role of Exact Exchange. *J. Chem. Phys.* **1993**, *98*, 5648−5652.
(14) Lee, C.; Yang, W.; Parr, R. G. Development of the Colle-Salvetti Correlation-Energy Formula into a Functional of the Energy Density. *Phys. Rev. B: Condens. Matter Mater. Phys.* **1988**, *37*, 785−789.
(15) Vosko, S. H.; Wilk, L.; Nusair, M. Accurate Spin-Dependent Electron Liquid Correlation Energies for Local Spin-Density Calculations - a Critical Analysis. *Can. J. Phys.* **1980**, *58*, 1200−1211.
(16) Stephens, P. J.; Devlin, F. J.; Chabalowski, C. F.; Frisch, M. J. Ab Initio Calculation of Vibrational Absorption and Circular Dichroism Spectra Using Density Functional Force Fields. *J. Phys. Chem.* **1994**, *98*, 11623−7.
(17) Frisch, M. J.; Trucks, G. W.; Schlegel, H. B.; Scuseria, G. E.; Robb, M. A.; Cheeseman, J. R.; Scalmani, G.; Barone, V.; Mennucci, B.; Petersson, G. A.; et al. *Gaussian 09*, Revision D.01; Gaussian, Inc.: Wallingford CT, 2009.
(18) Schmider, H. L.; Becke, A. D. Optimized Density Functionals from the Extended G2 Test Set. *J. Chem. Phys.* **1998**, *108*, 9624−9631.
(19) Møller, C.; Plesset, M. S. Note on an Approximation Treatment for Many-Electron Systems. *Phys. Rev.* **1934**, *46*, 618−622.
(20) Adler, T. B.; Knizia, G.; Werner, H.-J. A Simple and Efficient CCSD(T)-F12 Approximation. *J. Chem. Phys.* **2007**, *127*, 221106.
(21) Knizia, G.; Adler, T. B.; Werner, H.-J. Simplified CCSD(T)-F12 methods: Theory and Benchmarks. *J. Chem. Phys.* **2009**, *130*, 054104.
(22) Dunning, T. H., Jr. Gaussian Basis Sets for use in Correlated Molecular Calculations. I. The Atoms Boron through Neon and Hydrogen. *J. Chem. Phys.* **1989**, *90*, 1007−23.
(23) Kendall, R. A.; Dunning, T. H., Jr.; Harrison, R. J. Electron Affinities of the First-Row Atoms Revisited. Systematic Basis Sets and Wave Functions. *J. Chem. Phys.* **1992**, *96*, 6796−806.
(24) Curtiss, L. A.; Redfern, P. C.; Raghavachari, K. Gaussian-4 Theory. *J. Chem. Phys.* **2007**, *126*, 084108.
(25) Werner, H.-J.; Knowles, P. J.; Knizia, G.; Manby, F. R.; Schütz, M. Molpro: a general-purpose quantum chemistry program package. *WIREs Comput Mol Sci* **2012**, *2*, 242.
(26) Werner, H. J.; Knowles, P. J.; Knizia, G.; Manby, F. R.; Schütz, M. Molpro: a General Purpose Quantum Chemistry Program Package. *Wiley Interdiscip. Rev.: Comput. Mol. Sci.* **2012**, *2*, 242−253.
(27) Glowacki, D. R.; Liang, C.-H.; Morley, C.; Pilling, M. J.; Robertson, S. H. MESMER: An Open-Source Master Equation Solver for Multi-Energy Well Reactions. *J. Phys. Chem. A* **2012**, *116*, 9545−9560.
(28) Coxon, J. A.; Foster, S. C. Radical Dependence of Spin-Orbit and L-Doubling Parameters in the X^2P Ground-State of Hydroxyl. *J. Mol. Spectrosc.* **1982**, *91*, 243−254.
(29) Craven, P. M.; Lambert, J. D. The Viscosities of Organic Vapours. *Proc. R. Soc. London, Ser. A* **1951**, *205*, 439−449.
(30) Chu, P. M.; Guenther, F. R.; Rhoderick, G. C.; Lafferty, W. J. Quantitative Infrared Database. In *NIST Chemistry WebBook*; Linstrom, P. J., Mallard, W. G., Eds.; NIST Standard Reference Database Number 69; National Institute of Standards and Technology: Gaithersburg MD, http://webbook.nist.gov (retrieved May 17, 2020).
(31) York, D. Least-Squares Fitting of a Straight Line. *Can. J. Phys.* **1966**, *44*, 1079−1086.
(32) McGillen, M. R.; Carter, W. P. L.; Mellouki, A.; Orlando, J. J.; Picquet-Varrault, B.; Wallington, T. J. Database for the Kinetics of the Gas-Phase Atmospheric Reactions of Organic Compounds. *Earth Syst. Sci. Data* **2020**, *12*, 1203−1216.
(33) Huber, K. P.; Herzberg, G. In *Molecular Spectra and Molecular Structure: IV. Constants of Diatomic Molecules*; Huber, K. P., Herzberg, G., Eds.; Springer US: Boston, MA, 1979; pp 8−689.
(34) Scarl, E. A.; Dalby, F. W. High-Field Stark Effects on the Near Ultraviolet Spectrum of the Hydroxyl Radical. *Can. J. Phys.* **1971**, *49*, 2825−32.
(35) *NIST Computational Chemistry Comparison and Benchmark Database*; Johnson, R. D., III, Ed; NIST Standard Reference Database Number 101. Release 20, August 2018; http://cccbdb.nist.gov (retrieved May 17, 2020).
(36) Ishiwata, T.; Tanaka, I.; Kawaguchi, K.; Hirota, E. Infrared Diode Laser Spectroscopy of the NO_3 ν_3 Band. *J. Chem. Phys.* **1985**, *82*, 2196−2205.
(37) Kawaguchi, K.; Hirota, E.; Ishiwata, T.; Tanaka, I. A Reinvestigation of the NO_3 1492 cm^{-1} Band. *J. Chem. Phys.* **1990**, *93*, 951−956.
(38) Eisfeld, W.; Morokuma, K. A Detailed Study on the Symmetry Breaking and its Effect on the Potential Surface of NO_3. *J. Chem. Phys.* **2000**, *113*, 5587−5597.
(39) Antonsen, S. G.; Bunkan, A. J. C.; Mikoviny, T.; Nielsen, C. J.; Stenstrøm, Y.; Wisthaler, A.; Zardin, E. Atmospheric Chemistry of Diazomethane − an Experimental and Theoretical Study. *Mol. Phys.* **2020**, 1−8.
(40) Chase, M. W. NIST-JANAF Thermochemical Tables, Fourth Edition, Monograph 9 (Part I and Part II). *J. Phys. Chem. Ref. Data* **1998**.
(41) Jacox, M. E. Vibrational and Electronic Energy Levels of Polyatomic Transient Molecules. *J. Phys. Chem. Ref. Data* **2003**, *32*, 1 DOI: 10.1063/1.1497629.
(42) Kawaguchi, K.; Ishiwata, T.; Hirota, E.; Tanaka, I. Infrared Spectroscopy of the NO_3 Radical. *Chem. Phys.* **1998**, *231*, 193−198.
(43) Tyuterev, V. G.; Tashkun, S.; Jensen, P.; Barbe, A.; Cours, T. Determination of the Effective Ground State Potential Energy Function of Ozone from High-Resolution Infrared Spectra. *J. Mol. Spectrosc.* **1999**, *198*, 57−76.
(44) Mack, K. M.; Muenter, J. S. Stark and Zeeman Properties of Ozone from Molecular Beam Spectroscopy. *J. Chem. Phys.* **1977**, *66*, 5278−5283.
(45) Pickett, H. M.; Cohen, E. A.; Brown, L. R.; Rinsland, C. P.; Smith, M. A. H.; Devi, V. M.; Goldman, A.; Barbe, A.; Carli, B.; Carlotti, M. The Vibrational and Rotational Spectra of Ozone for the (0, 1, 0) and (0, 2, 0) States. *J. Mol. Spectrosc.* **1988**, *128*, 151−171.
(46) Flaud, J. M.; Camy-Peyret, C.; Devi, V. M.; Rinsland, C. P.; Smith, M. A. H. The ν_1 and ν_3 Bands of $^{16}O_3$: Line Positions and Intensities. *J. Mol. Spectrosc.* **1987**, *124*, 209−217.
(47) Kucharski, S. A.; Bartlett, R. J. Connected Quadruples for the Frequencies of O_3. *J. Chem. Phys.* **1999**, *110*, 8233−8235.
(48) Margulès, L.; Demaison, J.; Rudolph, H. D. Ab Initio and Experimental Structures of CH_3NC. *J. Mol. Struct.* **2001**, *599*, 23−30.
(49) Ghosh, S. N.; Trambarulo, R.; Gordy, W. Electric Dipole Moments of Several Molecules from the Stark Effect. *J. Chem. Phys.* **1953**, *21*, 308−310.

https://dx.doi.org/10.1021/acs.jpca.0c05127
J. Phys. Chem. A 2020, 124, 6562−6571

(50) Shimanouchi, T. *Tables of Molecular Vibrational Frequencies Consolidated Vol. I*; National Bureau of Standards: Washington, DC, 1972.
(51) Lee, T. J.; Taylor, P. R. A Diagnostic for Determining the Quality of Single-Reference Electron Correlation Methods. *Int. J. Quantum Chem.* **1989**, *36*, 199−207.
(52) Janssen, C. L.; Nielsen, I. M. New diagnostics for coupled-cluster and Møller−Plesset perturbation theory. *Chem. Phys. Lett.* **1998**, *290*, 423−430.
(53) Lee, T. J. Comparison of the T_1 and D_1 Diagnostics for Electronic Structure Theory: a new Definition for the Open-Shell D1 Diagnostic. *Chem. Phys. Lett.* **2003**, *372*, 362−367.
(54) Georgievskii, Y.; Klippenstein, S. J. Long-Range Transition State Theory. *J. Chem. Phys.* **2005**, *122*, 194103.
(55) Miller, W. H. Tunneling Corrections to Unimolecular Rate Constants, with application to Formaldehyde. *J. Am. Chem. Soc.* **1979**, *101*, 6810−6814.
(56) Wayne, R. P.; Barnes, I.; Biggs, P.; Burrows, J. P.; Canosamas, C. E.; Hjorth, J.; Lebras, G.; Moortgat, G. K.; Perner, D.; Poulet, G.; et al. The Nitrate Radical - Physics, Chemistry, and the Atmosphere. *Atmos. Environ., Part A* **1991**, *25A*, 1−203.
(57) Atkinson, R. Kinetics and Mechanisms of the Gas-Phase Reactions of the NO_3 Radical with Organic Compounds. *J. Phys. Chem. Ref. Data* **1991**, *20*, 459−507.
(58) Roberts, J. M.; Liu, Y. Solubility and Solution-Phase Chemistry of Isocyanic Acid, Methyl Isocyanate, and Cyanogen Halides. *Atmos. Chem. Phys.* **2019**, *19*, 4419−4437.
(59) Papanastasiou, D. K.; Bernard, F.; Burkholder, J. B. Atmospheric Fate of Methyl Isocyanate, CH_3NCO: OH and Cl Reaction Kinetics and Identification of Formyl Isocyanate, HC(O)-NCO *ACS Earth and Space Chem.* **2020**, submitted (sp-2020-001574).

NOTE ADDED AFTER ASAP PUBLICATION

This paper was published ASAP on July 30, 2020. Due to production error, part of the Figure 6 graphic was missing. The corrected version was reposted on August 5, 2020.

https://dx.doi.org/10.1021/acs.jpca.0c05127
J. Phys. Chem. A 2020, 124, 6562−6571